Ocean Engineering 195 (2020) 106716

Contents lists available at ScienceDirect

Ocean Engineering

journal homepage: www.elsevier.com/locate/oceaneng

# Evaluation of different earthquake scaling relations on the generation of tsunamis and hazard assessment

Zhisong Li, Chao An *, Hua Liu

*Key Laboratory of Hydrodynamics (Ministry of Education), School of Naval Architecture, Ocean and Civil Engineering, Shanghai Jiao Tong University, Shanghai, China*

ARTICLE INFO

*Keywords:*
Tsunamis
Tsunami warning
Scaling relations

ABSTRACT

Earthquake source details can hardly be determined accurately in a short time window after an earthquake. For rapid tsunami warning purposes, rupture parameters for a given earthquake magnitude are estimated using empirical scaling relations. In this paper, we evaluate the effectiveness of several commonly-used scaling relations. It is found that, for the 2011 Tohoku earthquake, most scaling relations overestimate the rupture area and underestimate the average rupture slip, resulting in predictions of earlier wave arrivals and smaller wave amplitudes in comparison to recordings. The scaling relation that uses "asperity size" instead of actual rupture area, presents a smaller rupture area and a larger average slip, leading to better tsunami predictions. While for the 2014 Iquique and 2015 Illapel tsunamis of relatively smaller earthquake magnitude, different scaling relations lead to comparable tsunami predictions. We further implement these scaling relations to study a potential earthquake in the Manila subduction zone. Results show that different scaling relations cause significant differences in the tsunami arrival time and wave amplitude at coastal cities, especially in the along-trench direction. Thus, to access the tsunami threat from mega-earthquakes and build early warning systems, it is necessary to select the appropriate scaling relations.

## 1. Introduction

Most devastating tsunamis in history are caused by thrust earthquakes in subduction zones, leading to severe damage to the coastal community, such as the 1960 $M_w$ 9.5 Chile earthquake (Cisternas et al., 2005), the 1964 $M_w$ 9.2 Alaska earthquake (Reimnitz and Marshall, 1965; Ichinose et al., 2007), the 2004 $M_w$ 9.1 Sumatra earthquake (Lay et al., 2005; Titov et al., 2005), the 2011 $M_w$ 9.1 Tohoku earthquake (Simons et al., 2011; Fujii et al., 2011; Satake et al., 2013), and two recent Chilean tsunamis in 2014 and 2015. The 2014 Iquique earthquake occurred in the northern portion of the 1877 earthquake seismic gap in northern Chile. Slip deficit of about 6 to 9 m may have accumulated since 1877. Post-event analysis of tsunami records shows that the shallow rupture near the trench is very small (Lay et al., 2014; An et al., 2014), which may otherwise cause significantly larger tsunamis, as is the case for the Tohoku event. The 2015 Illapel tsunami was recorded by more than 20 gauges, but most of the gauges were located along the coastline. As a result, studies show large variance in the east–west location of the fault rupture, and it is still not clearly understood if there was significant shallow rupture near the trench (Tilmann et al., 2016; Li et al., 2016; Melgar et al., 2016; An et al., 2017; An and Meng, 2017).

For the most recent tsunamis, in light of the deployment of seismometers, tsunami buoys and other types of sensors, various data of the earthquakes and tsunamis are recorded, and they can be utilized to infer the earthquake rupture process and source parameters. In particular, the Deep-ocean Assessment and Reporting of Tsunami (DART) project provides real-time tsunami measurements in the open ocean. Including such data in finite-fault inversions can promisingly recover the tsunami source and reproduce the tsunami recordings (Satake, 1987; Fujii et al., 2011; Satake et al., 2013; An et al., 2014; Heidarzadeh et al., 2016; An et al., 2017). On such basis, for early tsunami warning purposes, the Pacific Tsunami Warning Centre (PTWC) conducts finite-fault inversions by making use of the DART data, and issues accurate tsunami predictions (Wei et al., 2003, 2008). However, in areas where there lacks tsunami buoys, such as the South China Sea, tsunami measurements are not available. As a result, most local tsunami warning systems rely on a different approach, which is called the tsunami scenario strategy. In such a strategy, for subduction zones with potential tsunami genesis, uniform slip models are constructed before an earthquake occurs, and the corresponding tsunamis are numerically simulated. After an earthquake, tsunami warnings are issued based on the scenario with the most similar earthquake magnitude. To construct

* Corresponding author.
*E-mail address:* anchao@sjtu.edu.cn (C. An).

https://doi.org/10.1016/j.oceaneng.2019.106716
Received 18 June 2019; Received in revised form 4 October 2019; Accepted 10 November 2019
Available online 13 November 2019

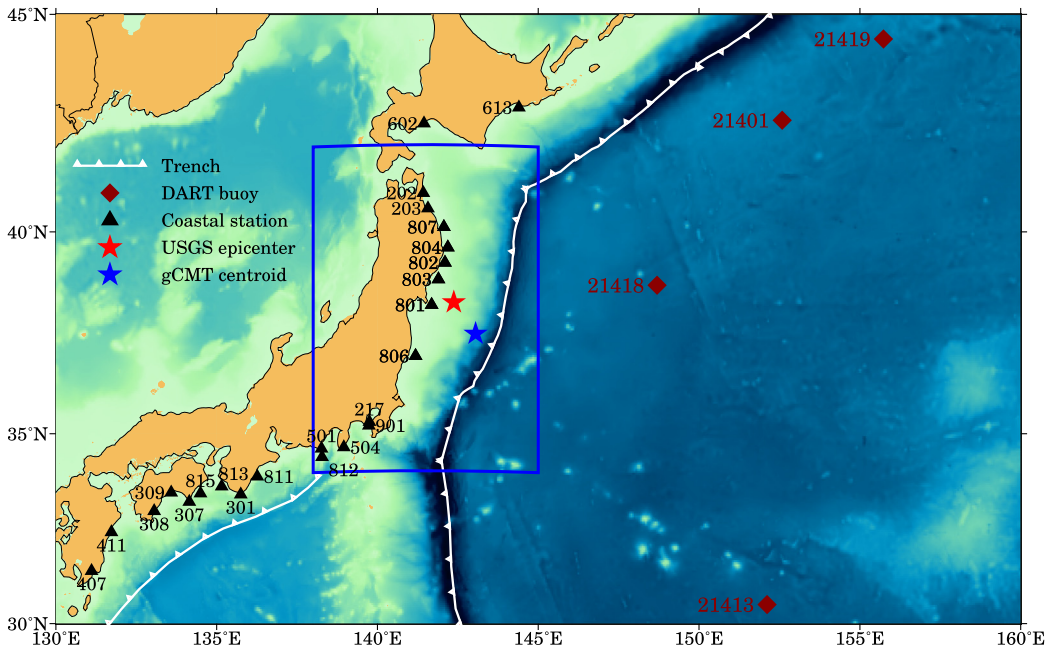


**Fig. 1.** Location of the tsunami gauges during the 2011 Tohoku event. The red and blue stars show the United States Geological Survey (USGS) epicenter and the centroid of global Centroid Moment Tensor (gCMT) solution (Ekström et al., 2012), respectively. The dark red diamonds indicate the DART buoy stations. The black triangles denote the coastal stations, which include GPS buoys, seabed wave gauges and coastal tide gauges (Kawai et al., 2013). The initial sea surface deformation in the blue rectangular is displayed in Fig. 3a. (For interpretation of the references to color in this figure legend, the reader is referred to the web version of this article.)

the uniform slip models, fault rupture parameters are obtained from a given earthquake magnitude according to empirical scaling relations (Wells and Coppersmith, 1994; Blaser et al., 2010; Strasser et al., 2010; Murotani et al., 2008, 2013; Thingbaijam et al., 2017).

Tsunami sources in reality involve temporal processes regarding earthquake ruptures. For example, Ren et al. (2019) evaluated the impact of kinetic rupture on tsunami generation and propagation during the 2004 Sumatra and 2011 Tohoku tsunamis. However, tsunami warning systems ignore such effects for the purpose of rapid warning. Scaling relations provide a quantitative relationship between rupture parameters (e.g., length, width, slip) and earthquake magnitude. They are usually derived from the regression of large databases of historical earthquakes. Due to the different database used and different type of earthquakes, studies often obtain similar but slightly different scaling relations. For instance, Wells and Coppersmith (1994) compiled the source parameters of 244 global earthquakes, classified them according to their focal mechanism, and derived scaling relations for different types of earthquakes. Even though the moment magnitude of earthquakes ranges $M_w$ 5 ~ 8 in their study, the scaling relations obtained for thrust earthquakes have been widely used to access the tsunami hazards for magnitude 8 or larger earthquakes (Liu et al., 2009; Wu and Huang, 2009; Nguyen et al., 2014). Blaser et al. (2010) extended the earthquake catalog adopted by Wells and Coppersmith (1994) from 244 to 283 earthquakes, by adding more subduction earthquakes of relatively higher moment magnitude (up to $M_w$ 9.5). They derived a new set of scaling relations with special focus on the large subduction zone earthquakes. Strasser et al. (2010) obtained similar scaling relations as Blaser et al. (2010)'s, by compiling 95 inter-plate earthquakes in addition to Wells and Coppersmith (1994)'s earthquake catalogue, with magnitude ranging from $M_w$ 6.3 to $M_w$ 9.4. Murotani et al. (2008, 2013) collected the finite-fault slip models of plate-boundary earthquakes ($M_w$ 6.7 ~ 9.2) in the vicinity of Japan that occurred from 1923 to 2011, and derived a scaling relation between the conventional rupture area $S$ and the seismic moment $M_0$. Particularly, they also proposed a scaling relation between the asperity rupture area $S_a$ and the seismic moment, where $S_a$ is defined as the fault area with slip 1.5 times the average slip or larger. A most recent study by Thingbaijam et al. (2017) observed that the scaling behavior of the rupture area to moment is consistent for all cases except normal-faulting earthquakes.

Empirical scaling relations are widely used to assess regional tsunami hazards (Liu et al., 2009; Wu and Huang, 2009; Nguyen et al., 2014; Ren et al., 2017). In addition, local tsunami warning systems also depend on such scaling relations. For instance, the South China Sea tsunami warning system operated by National Marine Environment Forecasting Center (China) adopts the scaling relations given by Wells and Coppersmith (1994) and Ren et al. (2014). The Japan tsunami warning system operated by the Japan Meteorological Agency (JMA) (Kamigaichi, 2009) uses the following scaling relations: $\log L = 0.5M_w - 1.8$ and $L = 2W$ ($L$ rupture length, $W$ rupture width, $M_w$ earthquake magnitude). It should be noted that most of these scaling relations are derived from seismic data. There have been very few studies that quantitatively evaluate their effectiveness in generating tsunamis. In a most recent study, An et al. (2018) demonstrated that slip heterogeneity can largely be ignored for tsunami warning purposes, and they also derived a scaling relation suitable for tsunami generation.

In this study, we test the performance of four representative and commonly-used scaling relations, given by Wells and Coppersmith (1994) (hereafter referred to as Wells1994), Blaser et al. (2010) (hereafter Blaser2010), Strasser et al. (2010) (hereafter Strasser2010) and Murotani et al. (2013) (hereafter Murotani2013) respectively, by applying them to the 2011 Tohoku, 2014 Iquique and 2015 Illapel tsunamis. Stirling et al. (2013) compiled a worldwide set of scaling relations and evaluated their relevance to a range of tectonic regimes. They pointed out that the Wells1994 scaling relations are out of date in terms of data and hence should not be used if more modern scaling relations are available. However, since the Wells1994 scaling relations are still widely adopted by tsunami modelers, it is included in the analysis of this study. The results of Strasser2010 are found to be very similar to that of Blaser2010, so it is excluded from the main text but provided in the supplementary information and discussed in the discussion section. The numerically simulated tsunami waves from scaling relations are compared to the tsunami recordings at various sensors. South China Sea has drawn many research interests due to its potential of large tsunamis, and a local warning system is in need (Lin et al., 2015). Thus,

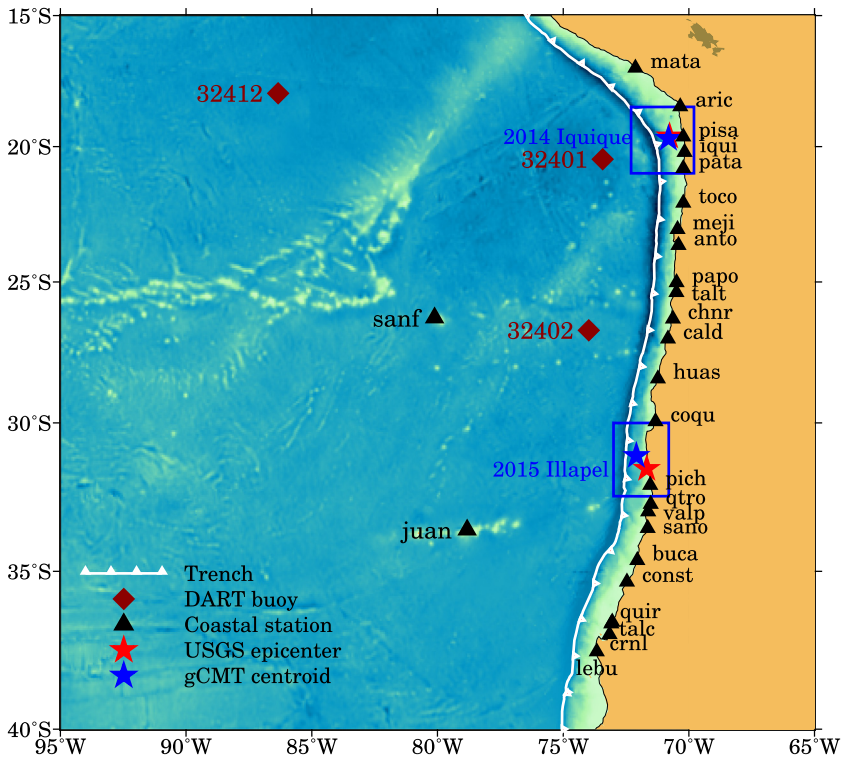


**Fig. 2.** Location of the tsunami gauges during the 2014 Iquique and 2015 Illapel earthquakes. The initial sea surface deformation in the blue rectangles is displayed in Fig. 3b and 3c.

**Table 1**
Fault parameters for the 2011 Tohoku, the 2014 Iquique and the 2015 Illapel earthquakes. 2011 Tohoku: $M_0 = 2.25 \times 10^{22}$ Nm ($M_w$8.9); 2014 Iquique: $M_0 = 1.22 \times 10^{21}$ Nm ($M_w$8.0); 2015 Illapel: $M_0 = 2.46 \times 10^{21}$ Nm ($M_w$8.2).

| Scenario | Event | Length (km) | Width (km) | Slip (m) | Reference |
|---|---|---|---|---|---|
| Wells1994 | Tohoku | 557 | 96 | 10.33 | Wells and Coppersmith (1994) |
| | Iquique | 158 | 48 | 4.48 | $\log S = -3.99 + 0.98 M_w$ |
| | Illapel | 210 | 56 | 5.05 | $\log L = -2.68 + 0.63 M_w$ |
| Blaser2010 | Tohoku | 504 | 171 | 6.44 | Blaser et al. (2010) |
| | Iquique | 161 | 68 | 3.09 | $\log L = -2.37 + 0.57 M_w$ |
| | Illapel | 209 | 84 | 3.75 | $\log W = -1.80 + 0.45 M_w$ |
| Murotani2013 | Tohoku | 155 | 155 | 23.12 | Murotani et al. (2013) |
| | Iquique | 57 | 57 | 10.45 | $S_a = 2.81 \times 10^{-11} M_0^{2/3}$ |
| | Illapel | 72 | 72 | 12.91 | $S_a = L \times W$, $L = W$ |

$M_w = \frac{2}{3} \log M_0 - 10.7$. $M_w$ is the earthquake magnitude and $M_0$ is the earthquake moment.

we apply the three scaling relations in a virtual earthquake scenario of $M_w$ 9.0 in the Manila subduction zone. Tsunami arrival time and wave heights are analyzed near the coastlines surrounding the South China Sea, which will be useful for future design of tsunami warning systems.

## 2. Rupture parameters from different scaling relations

We select three well-documented tsunami events to evaluate the effectiveness of different scaling relations on the generation of tsunamis. They are the 2011 Tohoku earthquake (Fig. 1), the 2014 Iquique and the 2015 Illapel earthquakes (Fig. 2). The scaling relations adopted in this study are those given by Wells and Coppersmith (1994), Blaser et al. (2010) and Murotani et al. (2013). The source parameters derived from these scaling relations for the three earthquakes are shown in Table 1. The seismic moment for the three earthquakes is obtained from finite-fault inversions of tsunami data. It is $2.25 \times 10^{22}$ Nm ($M_w$ 8.9) for the 2011 Tohoku earthquake (An et al., 2018), $1.22 \times 10^{21}$ Nm ($M_w$ 8.0) for the 2014 Iquique earthquake (An et al., 2014), and $2.46 \times 10^{21}$ Nm ($M_w$ 8.2) for the 2015 Illapel earthquake (An et al., 2017), respectively. We note here that, for each earthquake event, we use the scaling relations to calculate the rupture dimension first (rupture area $S$, length $L$ and width $W$), and the average slip $D$ is then calculated by $M = \mu SD$ ($M$ seismic moment, $\mu$ Earth rigidity). The Earth rigidity used in this study, which varies in depth, is extracted from the Preliminary Reference Earth Model (PREM) (Dziewonski and Anderson, 1981). Murotani et al. (2013) provided two different scaling relations to the earthquake moment, regarding the conventional rupture area and the asperity size respectively. Here we use the formulas regarding the asperity size. In addition, the ratio of rupture length and width is not given by Murotani et al. (2013), and here we use a ratio of 1.0, which is found to be the optimum ratio for tsunami generation (An et al., 2018). Other ratios have also been addressed, and the results are given in the supplementary information. More discussions about the conventional rupture area and different length/width ratios are provided in the discussion section.

For the 2011 Tohoku earthquake, we assume a single fault plane with a strike angle of 198° and dip angle of 14° (Fujii et al., 2011). For the 2014 Iquique and the 2015 Illapel earthquakes, the strike angle is 340° and 4°, respectively; and the dip angle is extracted from the local slab geometry (Slab 1.0) (Hayes et al., 2012). The rake angle is set to 90° to represent thrust focal mechanism. The center of each rupture

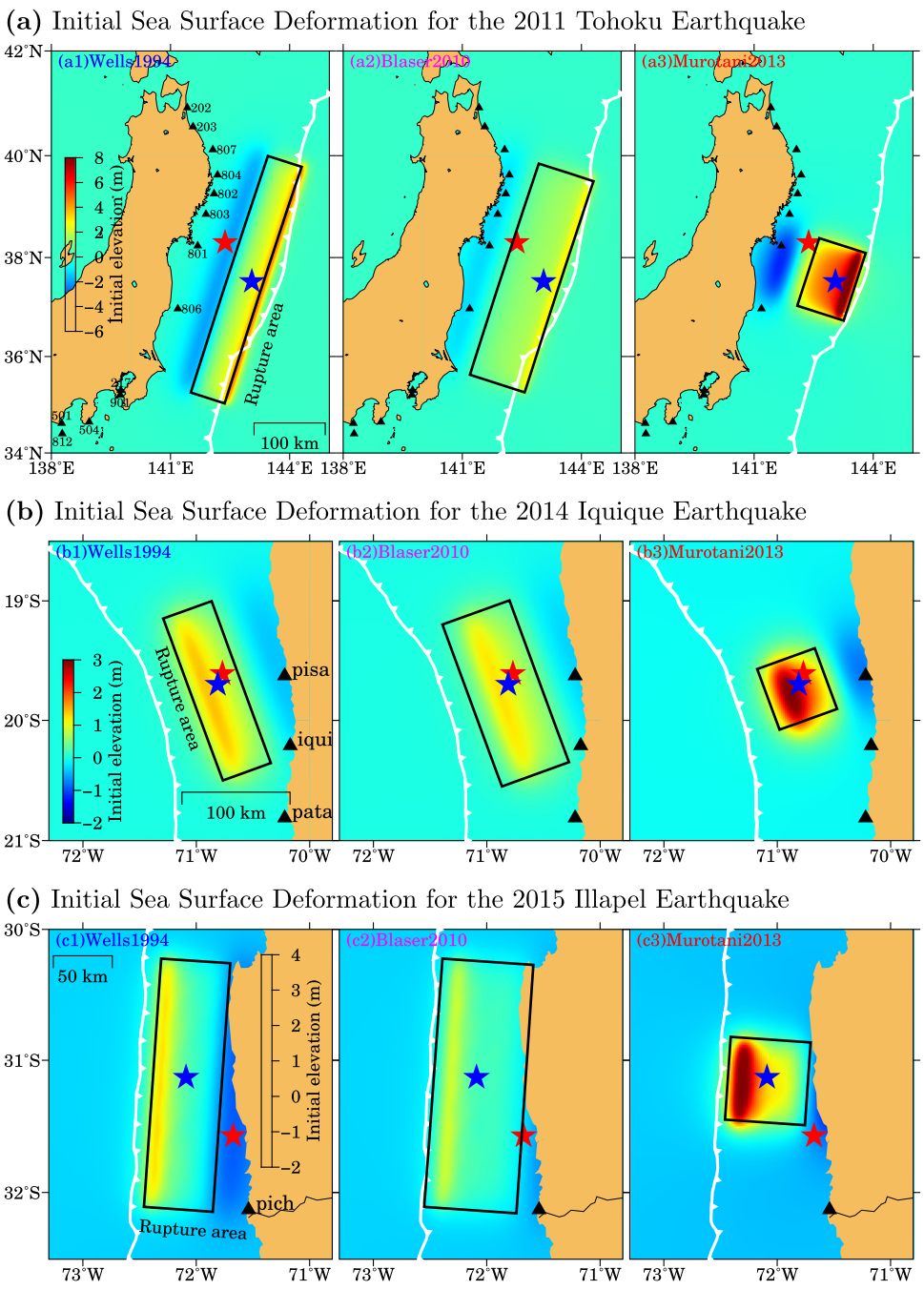


**Fig. 3.** Initial sea surface deformation for the 2011 Tohoku, 2014 Iquique and 2015 Illapel earthquakes. The red and the blue stars show the USGS epicenter and the gGMT centroid, respectively. The black rectangles denote the rupture areas with length and width given in Table 1. (For interpretation of the references to color in this figure legend, the reader is referred to the web version of this article.)

model is located at the global CMT centroid, which is derived from long-period seismic waves and may better represent the location of the final slip than the epicenter (An et al., 2018). All the fault parameters are provided in the supplementary information.

By applying the Okada's analytical solution (Okada, 1985) to the source parameters, the static seafloor deformation is calculated. And the corresponding initial sea surface elevation mimics the seafloor profile upon the assumption of instant rupture and incompressible water. The propagation of tsunami waves is then numerically simulated using the software package FUNWAVE-TVD (Shi et al., 2012; Kirby et al., 2013), which solves nonlinear Boussinesq equations. The computational domain for the 2011 Tohoku tsunami extends from 127°E to 160°E, 27.5°N to 47.5°N, and the total grid number is 3960 × 2400. The computational domain for the 2014 Iquique tsunami extends from 90°W to 65°W, 30°S to 15°S, and the total grid number is 3000 × 1800. The computational domain for the 2015 Illapel tsunami extends from 85°W to 65°W, 40°S to 15°S, and the total grid number is 2400 × 3000. The global bathymetry data GEBCO 2014 (General Bathymetric Chart of the Oceans, www.gebco.net) with a uniform resolution of 30 arcsec are used. We have carried out convergence tests using the Murotani2013 model for each tsunami event, with grid sizes of 90, 60 and 30 arcsec, respectively. The results are provided in Figs. S1, S2 and S3 for the Tohoku, Iquique and Illapel earthquakes, respectively. It is seen that 30 arcsec is sufficiently good for simulations of the tsunami waves at DART stations in deep water, and the first waves at most of the coastal stations. We point out that the bathymetry resolution of 30 arcsec

could be too coarse to resolve the complex local bathymetry features at some coastal gauges, but at most stations the tsunami waves can be well modeled using grid size of 30 arcsec (e.g., Heidarzadeh et al., 2016; Melgar et al., 2016; An et al., 2017). The Courant–Friedrichs–Lewy (C.F.L.) number in the simulation is 0.5. The coefficient of bottom friction is 0.015. Sponge layers are imposed to absorb reflected wave at the computational boundaries, and the thickness of the sponge layers is 200 km.

## 3. Comparison of tsunami waveforms with observations

We first compare the initial sea surface deformation resulted from the three different scaling relations, shown in Fig. 3. For all the three earthquakes, it is observed that the Wells1994 scaling relations lead to narrow and long rupture areas. Due to the selected length/width ratio of 1.0, the rupture areas from the Murotani2013 scaling relations are concentrated in square zones. Results of different ratios are discussed in the discussion section. Consequently, the initial sea surface elevation is also narrow and long for the Wells1994 models, and relatively short for the Murotani2013 models. Besides, for the same earthquake, the rupture area is estimated to be larger using the Wells1994 scaling relations than using the Murotani2013 scaling relations. And the maximum initial wave height is therefore smaller in the Wells1994 models than in the Murotani2013 models. For all the three earthquakes, the Blaser2010 scaling relations lead to even larger rupture area and smaller maximum initial wave height than the Wells1994 models, albeit still very similar to the results of Wells1994.

We then compare the tsunami waves generated from the three slip models with recordings at various stations. The location of the DART buoys and coastal stations is given in Fig. 1 for the 2011 Tohoku event, and Fig. 2 for the 2014 Iquique and 2015 Illapel events. The comparison of tsunami waves is shown in Figs. 4–6 for the 2011 Tohoku, 2014 Iquique and 2015 Illapel event, respectively.

It is seen from the top panel of Fig. 4 that, for the 2011 Tohoku earthquake, the models of Wells1994 and Blaser2010 predict much earlier wave arrivals than the recordings at stations to the north and south of the earthquake source, such as stations 613, 202 and 203 in the north, stations 407, 815 and 812 in the south. This is due to the elongated rupture area estimated using the scaling relations of Wells1994 and Blaser2010 (Fig. 3a). On the other hand, the arrival time predicted by the Murotani2013 model is similar to the recordings at most of the stations. Besides, we also observe that the predicted wave heights by the Wells1994 and Blaser2010 models are smaller than recorded at most of the stations, while the predicted amplitudes by the Murotani2013 model agree well with the recordings. Thus, it can be inferred that the Wells1994 and Blaser2010 models underestimate the initial wave height, and the Murotani2013 model leads to initial wave height similar to reality. This is also demonstrated by the bottom panel of Fig. 4, which shows the relative error of the first-wave arrival time and amplitude predicted by the three slip models. At most stations, the Murotani2013 model produces clearly smaller errors than the other two models.

For the 2014 Iquique earthquake, shown in Fig. 5, it is found that the predictions from the three slip models present less significant differences compared to the 2011 Tohoku event. At some stations (e.g., mata, pata, toco, meji, anto), the results of Wells1994 and Blaser2010 have earlier wave arrivals and smaller first-wave amplitudes than the results of Murotani2013. However, the overall discrepancies are less observable than those in the 2011 Tohoku earthquake. This is also shown in the bottom panel of Fig. 5, which plots the relative error of first-wave arrival time and amplitude. The reason is that the magnitude of the 2014 Iquique earthquake is much smaller than the 2011 Tohoku earthquake, and hence the rupture dimension of the 2014 Iquique earthquake is also much smaller. Thus, the absolute differences of rupture dimension estimated from different scaling relations are also smaller, leading to smaller discrepancies of first-wave arrival time and amplitude.

For the 2015 Illapel earthquake, the magnitude is smaller than the 2011 Tohoku earthquake and larger than the 2014 Iquique earthquake. Therefore, the discrepancies among the three scaling relations are less significant than those in the 2011 Tohoku earthquake, and more significant than those in the 2014 Iquique earthquake, respectively. The results are shown in Fig. 6. From Figs. 4–6, it can be concluded that, the larger the earthquake magnitude, the more significant the discrepancies of tsunami waves predicted from different scaling relations. In addition, based on the results of the three investigated earthquakes, for earthquakes of larger magnitude, the scaling relations of Murotani2013 with a length/width ratio of 1.0 lead to better tsunami predictions than other scaling relations.

## 4. Assessment of potential megatsunamis near the manila trench

The Manila Trench is an oceanic trench along which the Eurasian plate is subducting eastward underneath the Luzon volcanic arc on the Philippine Sea Plate. There have been many studies to investigate its potential to produce large earthquakes and tsunamis. Galgana et al. (2007) utilized regional GPS velocities and focal mechanism data to constrain the tectonic deformation along the Manila subduction zone, and results suggested that the Manila trench could be possibly poorly coupled. Similarly, Hsu et al. (2012) used GPS data, trench parallel gravity anomaly and bathymetry to infer plate coupling patterns along the Manila subduction zone. They derived a maximum plate coupling ratio of 0.4 between the West Luzon Trough and the Scarborough Seamount, and concluded that megathrust rupture along the entire Manila subduction zone is not likely. Nevertheless, people are still concerned about mega earthquakes and tsunami in this zone. Liu et al. (2009), Megawati et al. (2009) and Nguyen et al. (2014) simulated the tsunami waves generated by earthquakes of various magnitudes near the Manila trench propagating to the coast of China, Vietnam and Philippine. Ren et al. (2015, 2017) and Li et al. (2018) investigated the characteristics of the evolution of tsunami waves over the mild slope in the South China Sea, including wave dispersion, nonlinearity and wave splitting. Liu et al. (2009) proposed a tsunami warning strategy based on finite-fault inversion theory. Most of the above-mentioned studies adopt uniform slip models to calculate the tsunami waves generated from an earthquake. The parameters of the uniform slip models are obtained from a given earthquake magnitude using different scaling relations. Here we quantify the impact of different scaling relations on the generated tsunami waves in the South China Sea, by numerically simulating an artificial earthquake and the following tsunami.

We artificially impose a giant earthquake on the fault of the Manila trench, with the same seismic moment as the 2011 Tohoku earthquake ($M_w$ 8.9). We point out that, the largest earthquake in the Manila subduction zone that caused a known tsunami in history had a magnitude of 7.9, which occurred on February 14, 1934 (NOAA, 2019). However, larger earthquakes could also possibly happen. For example, the magnitude of the 2011 Tohoku earthquake was not expected before the earthquake (Kido et al., 2011; Lay et al., 2011). Previous works have considered $M_w \sim 9$ or larger earthquakes in the Manila subduction zone (Wu and Huang, 2009; Megawati et al., 2009; Nguyen et al., 2014). The fault geometry is inferred from the earthquake focal mechanisms in the time period between 1973 and 2010 (Hsu et al., 2012), which consists of three major segments, with uniform strike angle and an averaged dip angle in depth for each segment. The artificial earthquake is located in the middle segment. The rupture dimension and average slip can be calculated using different scaling relations, and the results are the same as the Tohoku event, shown in Table 1. The focal depth is determined such that the top edge of the rupture area reaches the trench. Note that the strike angle in the models of Wells1994 and Blaser2010 varies in order to follow the curvature of the trench. All the fault parameters are provided in the

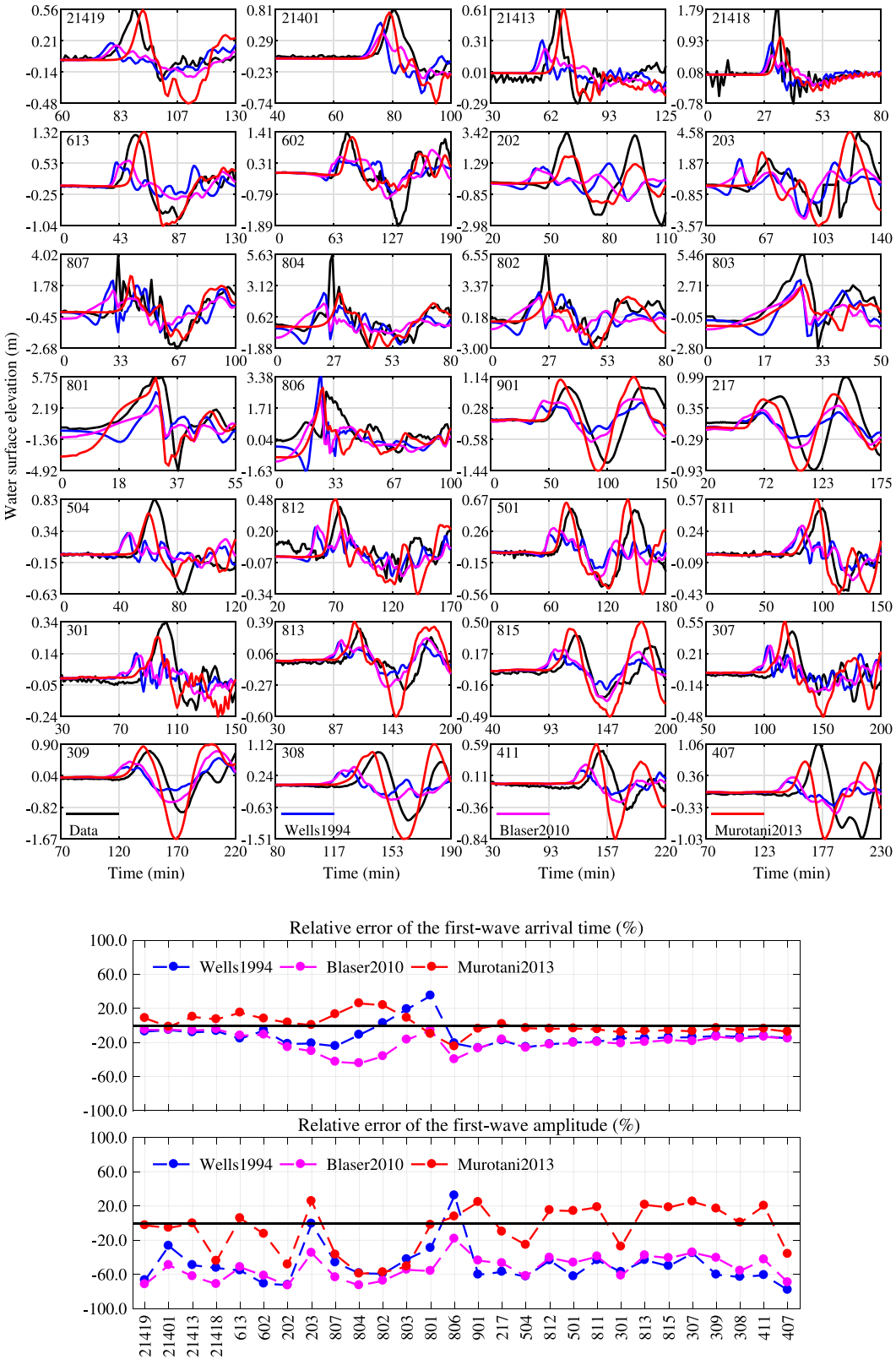


**Fig. 4.** Comparison of predicted and recorded tsunami waves during the 2011 Tohoku earthquake. Top panel: comparison of tsunami waveforms; bottom panel: relative errors of first-wave arrival time and amplitude.

supplementary information. We then simulate and analyze the tsunami waves propagating from the Manila trench to the surrounding countries (Fig. 7).

By adopting the half-space elastic dislocation model (Okada, 1985), the coseismic seafloor deformation and the initial water elevation are calculated, shown in the left panels of Fig. 8. Similar to the Tohoku

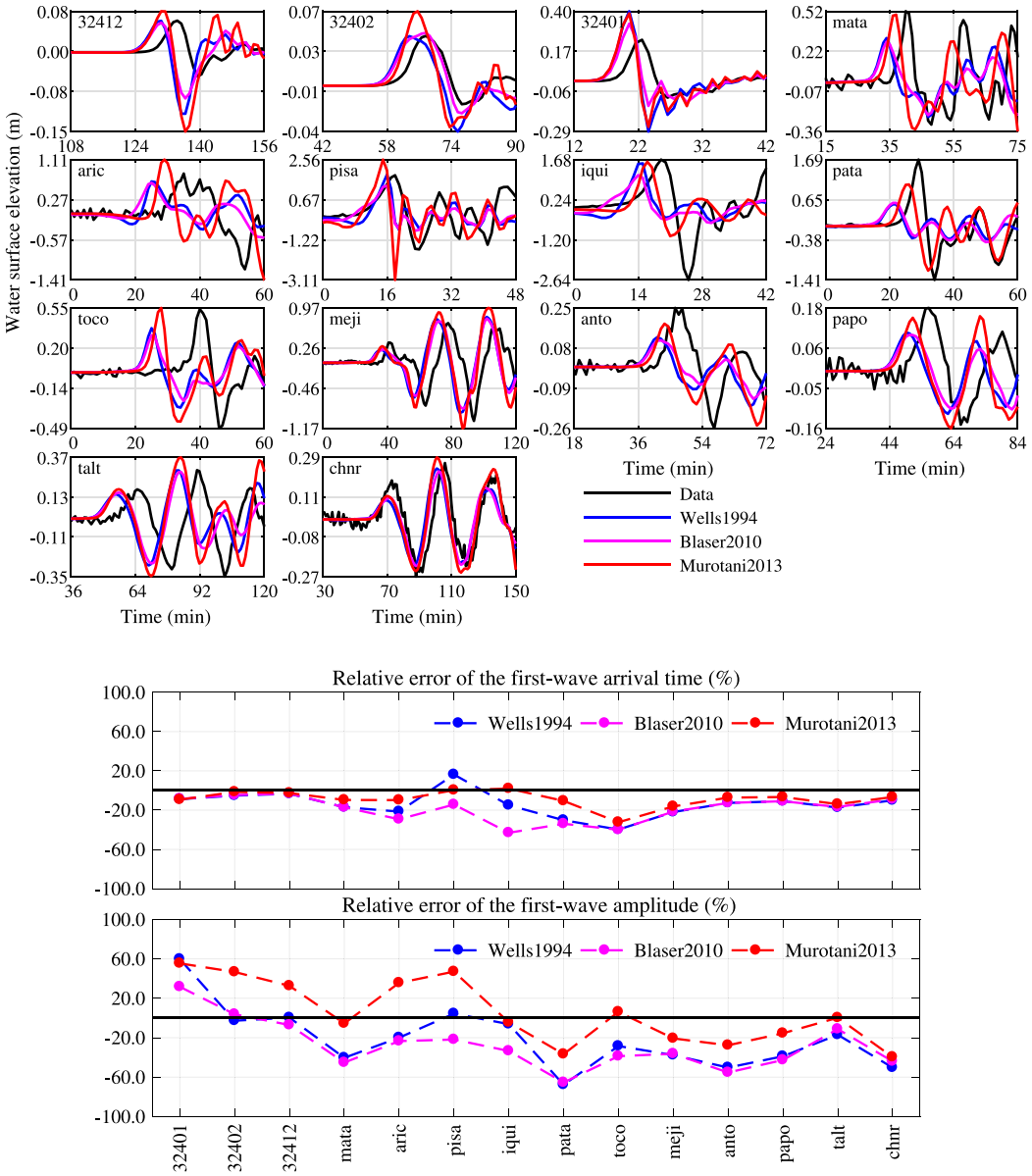


**Fig. 5.** Comparison of predicted and recorded tsunami waves during the 2014 Iquique earthquake. Top panel: comparison of tsunami waveforms; bottom panel: relative errors of first-wave arrival time and amplitude.

case, it is observed that the Wells1994 result presents an elongated zone of water elevation, and relatively small maximum wave height; while the Murotani2013 result shows a compact zone of relatively large wave height. The Blaser2010 model leads to an even larger area of water elevation with smaller wave height compared to the Wells1994 model. The right panels in Fig. 8 display the first-wave amplitude resulted from the three scaling relations. It is found that, in the direction perpendicular to the strike of the trench, where the tsunami energy is mostly concentrated, the Murotani2013 model impacts a wider area along the Chinese coast with higher wave height than the other two models. It seems to be the same for the coastal area along Vietnam and Taiwan, which is more clearly demonstrated in Fig. 9. We note here that the Wells1994 and Balser2010 models have curved strike direction, which can lead to different energy focusing compared to uniform strike. However, it is observed in Fig. 8 that the direction of energy concentration is still largely determined by the middle rupture zone.

Fig. 9 shows the simulated first-wave arrival time and amplitude along the coastlines surrounding the South China Sea. The top panel shows the results along the coastline of western Philippines, which is near the tsunami source. It is found that, although the Wells1994 model presents smaller maximum initial water height than the Murotani2013 model, the wave height along the coastline is somewhat larger. This is possibly because the Wells1994 model has a longer zone of water elevation extending to the south, so the coastline where the first-wave amplitude is analyzed is closer to the tsunami source. The second panel provides the results along the coastline of southern China, which is in the direction of tsunami energy focus. The arrival time is almost identical, because the edge of the initial water elevation starts from the trench in all the three models. The Murotani2013 model predicts large first-wave amplitude in a larger area than the Wells1994 model, while the Blaser2010 model leads to the smallest amplitude among the three models. In the third panel the first-wave arrival time and amplitude along the coastline of western Taiwan is plotted. Since the Murotani2013 model has a significantly smaller zone of tsunami source than the other two models, the arrival time is predicted to be clearly later. In addition, the first-wave amplitude given by the Murotani2013 model is also obviously larger, and it can be 1.5 to 2 times the amplitude predicted by the other two models. This is consistent with our

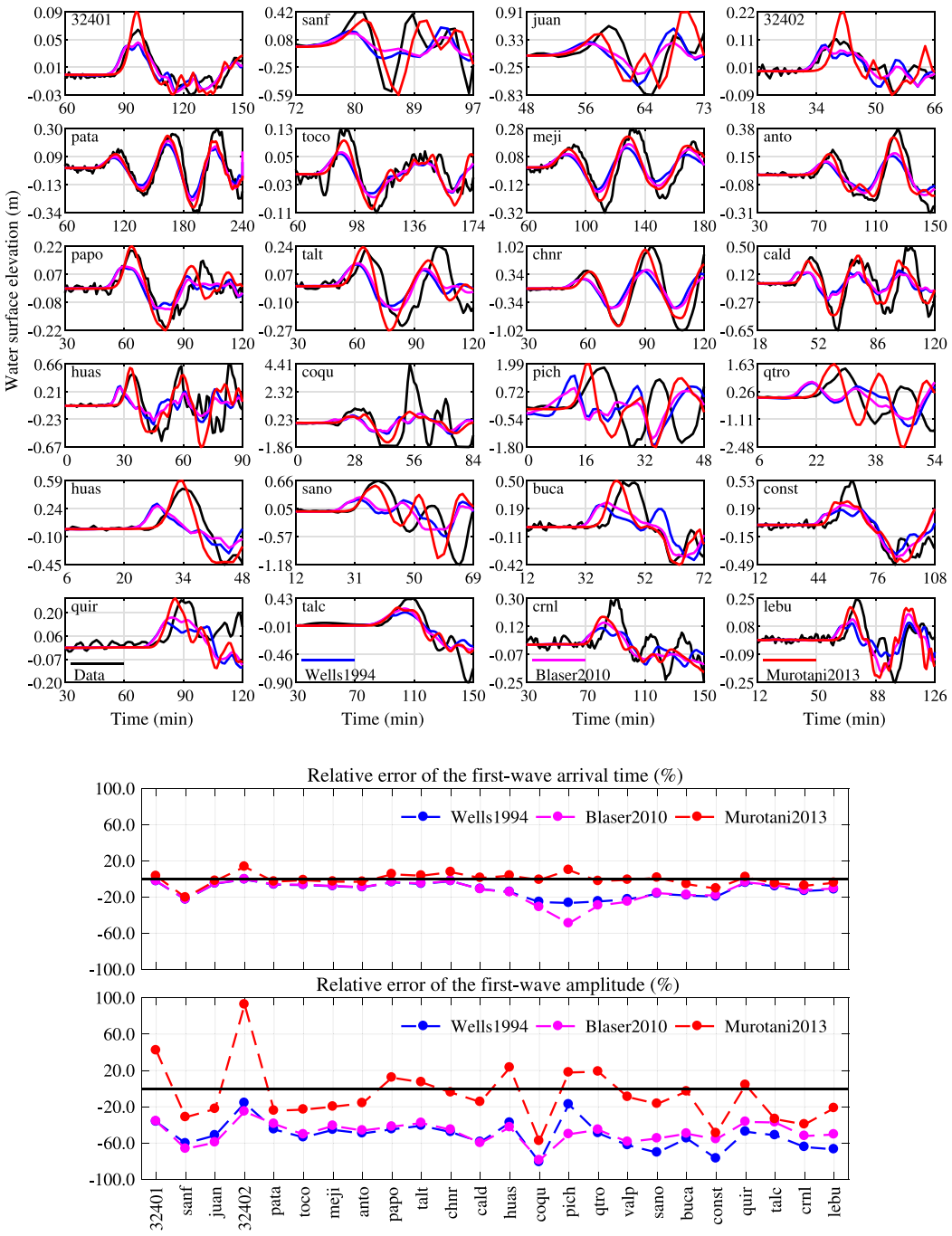


**Fig. 6.** Comparison of predicted and recorded tsunami waves during the 2015 Illapel earthquake. Top panel: comparison of tsunami waveforms; bottom panel: relative errors of first-wave arrival time and amplitude.

previous analysis of the Tohoku, Iquique and Illapel tsunamis. For the three previous tsunamis, most of the observation stations are located along the coast, which is parallel to the trench axis. In this synthetic test, Taiwan is also in the strike direction of the trench, where the Murotani2013 model predicts later arrival time and higher amplitude than the other two models. In the bottom panel of Fig. 9, along the coastline of western Vietnam, which is approximately parallel to the trench strike, the Murotani2013 model predicts slightly later first-wave arrivals and larger wave amplitude than the other two models.

## 5. Discussion

In the previous sections we have evaluated three scaling relations proposed by Wells and Coppersmith (1994), Blaser et al. (2010) and Murotani et al. (2013) on the generation of tsunami waves. Another widely-used scaling relation was derived by Strasser et al. (2010). Here we also analyze this scaling relation and compare the results with the three above-mentioned scaling relations. The results are found to be almost identical as the Blaser2010 results for all the three tsunami events. For example, for the Tohoku tsunami, the Blaser2010 model and Strasser et al.'s 2010 model lead to an averaged relative error of the first-wave arrival time of 20% and 21%, respectively, and an averaged relative error of the first-wave amplitude of 53% and 54%, respectively. Details are provided in the supplementary information (Tables S1, S2, Figs. S4, S5, S6, S7). Besides, in addition to the scaling relation regarding the "asperity size", Murotani et al. (2013) also obtained a scaling relation between the conventional rupture area and the

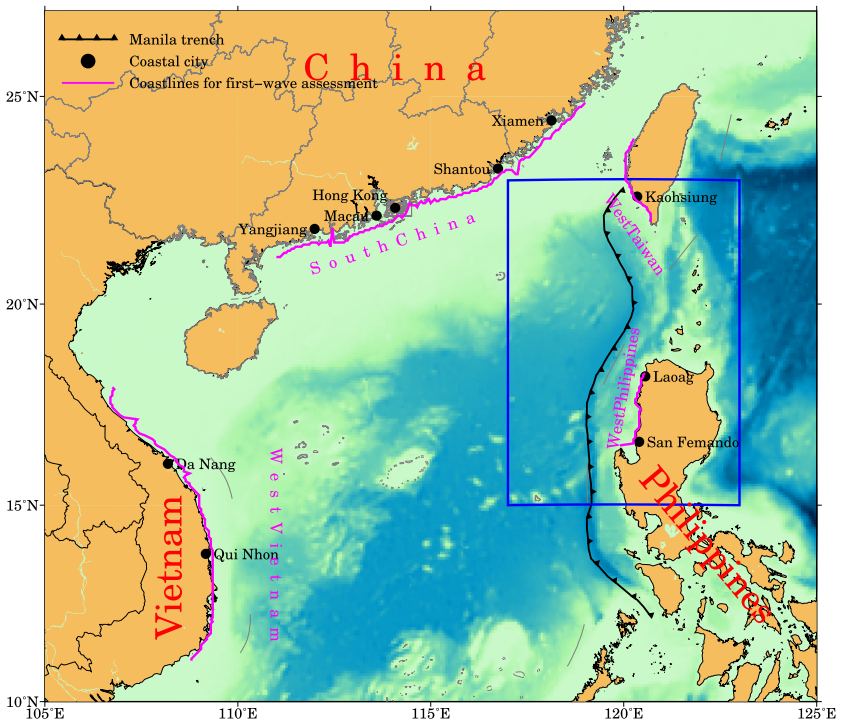


**Fig. 7.** The Manila subduction zone and the South China Sea. The blue rectangle encloses the potential source area, and the initial water elevation in this area from different scaling relations is calculated and shown in the left panels of Fig. 8. The four magenta lines indicate the 20 m depth contour near the coast, where the first-wave arrival time and amplitude from different scaling relations are compared, shown in Fig. 9. The computational domain extends from 98°E to 128°E, 0°N to 30°N, and the total grid number is 3600 × 3600.

earthquake magnitude. Hence we also adopt this scaling relation and simulate the tsunami waves for the Tohoku, Iquique and Illapel events. The results are found to be similar to the Blaser2010 results (Tables S3, S4, Figs. S8, S9, S10 and S11 in the supplementary information). Thus, although they vary in details, all the scaling relations including those given by Wells and Coppersmith (1994), Blaser et al. (2010), Strasser et al. (2010) and Murotani et al. (2013), produce comparable tsunami simulation results, except the one related to "asperity size" proposed by Murotani et al. (2013). Compared to other scaling relations, the Murotani2013 scaling relation regarding the asperity rupture area leads to smaller zone of initial water elevation with higher amplitude, resulting in later tsunami arrivals and larger first-wave amplitude near coastlines, especially in the direction of trench axis.

Murotani et al. (2013) provided only the scaling relation between the earthquake magnitude and the rupture area, without determining the rupture length/width ratio. In this study we adopt the length/width ratio of 1.0, which was found to be the optimum ratio for the three selected tsunamis by An et al. (2018). Here we also test a more widely-used value, 2.0, for the length/width ratio. The fault parameters with a length/width ratio of 2.0 are listed in Table S5, and the relative errors are given in Table S6. In Fig. S12, we observe that the results of ratio 2.0 have a more elongated zone of elevated water. Because most of the stations are located in the along-trench direction, the first-wave arrivals are earlier using ratio 2.0 than 1.0, as shown in Figs. S13, S14 and S15. Overall, the results of ratio 2.0 match the recordings worse than the results of ratio 1.0, which can also be seen from the arrival time and first-wave amplitude at observation stations. Besides, it is also found that the error of ratio 2.0 is more significant for the Tohoku event, and it decreases with the earthquake magnitude. This is attributed to the decrease of absolute rupture dimension. Table 2 summarizes the averaged relative errors of the first-wave amplitude and arrival time in the 2011 Tohoku, 2014 Iquique and 2015 Illapel tsunamis, using different scaling relations.

**Table 2**
Averaged relative errors of the first-wave amplitude and arrival time for the 2011 Tohoku, 2014 Iquique and 2015 Illapel tsunamis. Fault parameters for models Wells1994, Blaser2010 and Muotani2013 are listed in Table 1; fault parameters for models Stasser2010, Murotani2013c and Murotani2013R2 are listed in Tables S1, S3 and S5 in the supplementary information, respectively.

| Scenarios | First wave amplitude error (%) | | | Arrival time error (%) | | |
|---|---|---|---|---|---|---|
| | Tohoku | Iquique | Illapel | Tohoku | Iquique | Illapel |
| Wells1994 | 51 | 30 | 51 | 16 | 16 | 12 |
| Blaser2010 | 53 | 33 | 48 | 20 | 19 | 13 |
| Murotani2013 | 23 | 27 | 25 | 8 | 9 | 5 |
| Strasser2010 | 54 | 40 | 51 | 21 | 24 | 16 |
| Murotani2013c | 62 | 44 | 57 | 15 | 15 | 18 |
| Murotani2013R2 | 28 | 35 | 35 | 9 | 12 | 6 |

## 6. Conclusions

In this study, we evaluate the impact of scaling relations of earthquake source parameters on the generation of tsunamis. Four commonly-used scaling relations proposed by Wells and Coppersmith (1994), Blaser et al. (2010), Strasser et al. (2010) and Murotani et al. (2013) are studied by applying them to the 2011 Tohoku, 2014 Iquique, 2015 Illapel tsunamis. The resulted tsunami waves are compared with tsunami recordings at various observation stations. The main findings are summarized as follows.

- Wells and Coppersmith (1994), Blaser et al. (2010) and Strasser et al. (2010) predict relatively large source areas and small initial wave height, leading to early first-wave arrivals and small wave height, especially in the direction of trench axis.
- The scaling relation regarding the "asperity size" given by Murotani et al. (2013) produces a compact rupture area with relatively large initial water elevation, and the predicted tsunami waves match the recordings with significantly smaller errors in comparison to other scaling relations.

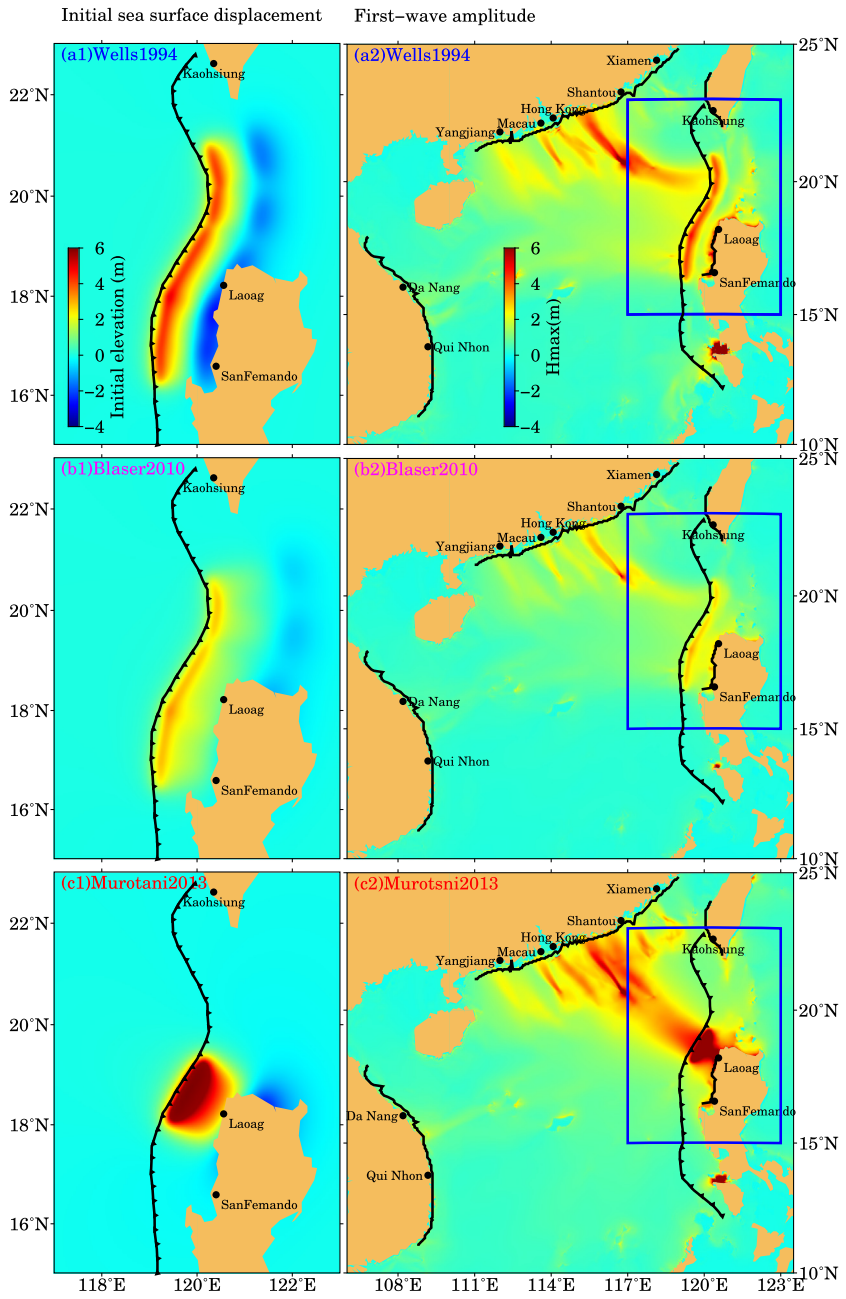


**Fig. 8.** The initial sea surface deformation and the maximum first-wave amplitude from the three scaling relations. The left panels show the initial water elevation and the right panels show the maximum first-wave amplitude.

- The discrepancies among the scaling relations are more significant for earthquakes of higher magnitude, e.g., the 2011 Tohoku earthquake, and less observable for smaller earthquakes, e.g., the 2014 Iquique earthquake.

For an artificial earthquake of magnitude $M_w \sim 9$ in the Manila subduction zone, different scaling relations also result in different tsunami simulation results.

- The largest discrepancies appear at the coastlines of western Taiwan. The arrival time predicted by the Murotani2013 scaling relation is significantly later, and the first-wave amplitude can be 1.5 to 2 times that given by the other scaling relations.
- Along the coastlines of western Vietnam and southern China, only part of the coastal area is affected by the different scaling relations.

As the United Nations Educational, Scientific and Cultural Organization (UNESCO) opened the South China Sea Tsunami Advisory Center in May 2018, which is now in operation to issue tsunami warnings for countries surrounding the South China Sea, it is important to choose an appropriate scaling relation in order for high prediction accuracy. We note that the conclusions are obtained based the three selected tsunamis. Recently it has been discussed that forcing the rupture area to be more compact than the conventional rupture area, such as the "asperity size" adopted by Murotani et al. (2013), could be a good practical solution to predict tsunami waves (Melgar et al., 2019). Slip on the fault during an earthquake is heterogeneous in reality. Thus, it reasonable that approximating the earthquake source using homogeneous slip should also require approximations of the rupture area. In this study we find that compact areas work well for the 2011 Tohoku,

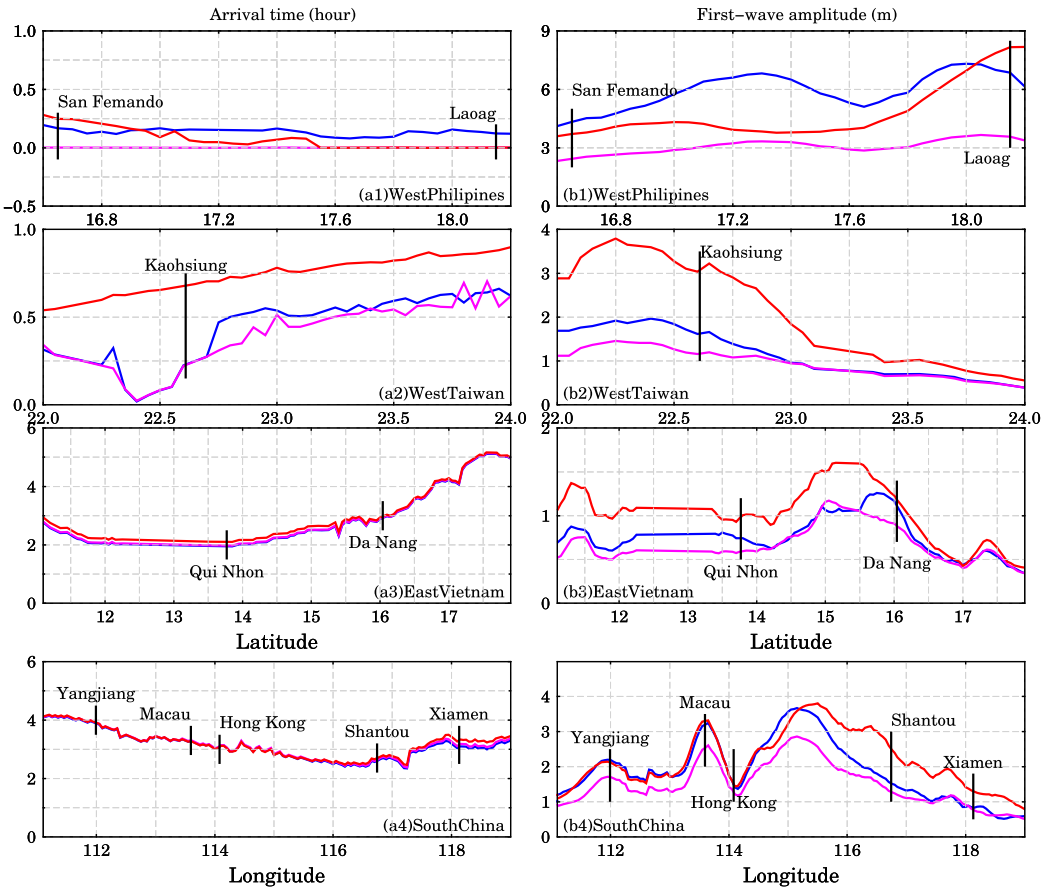


**Fig. 9.** First-wave arrival time and amplitude along the coastlines of western Philippines (top panel), southern China (second panel), eastern Vietnam (third panel) and western Taiwan (bottom panel). Blue lines denote the Wells1994 results, magenta lines indicate the Blaser2010 results and red lines show the Murotani2013 results. (For interpretation of the references to color in this figure legend, the reader is referred to the web version of this article.)

2014 Iquique and 2015 Illapel tsunamis, but further research might be necessary to verify if the conclusions apply to other tsunamis.

## Declaration of competing interest

The authors declare that they have no known competing financial interests or personal relationships that could have appeared to influence the work reported in this paper.

## Acknowledgments

This work is supported by the State's Key Project of Research and Development plan (China) grant 2016YFC1401506, the National Nature Science Foundation of China grant 11632012, 41861144024, and the 2018 Shanghai Pujiang Program (C. An). The tsunami data at DART stations were downloaded from NOAA's website (http://www.ndbc.noaa.gov/dart.shtml); the tsunami data at coastal stations during the 2011 Tohoku earthquake were downloaded from the Nationwide Ocean Wave Information Network for Ports Harbours, Japan (NOWPHAS, http://nowphas.mlit.go.jp/info_eng.html); the tsunami data at tide gauges during the 2014 Iquique and 2015 Illapel earthquakes were downloaded from the IOC's website (http://www.ioc-sealevelmonitoring.org). This work made use of the GMT software.

## Appendix A. Supplementary data

Supplementary material related to this article can be found online at https://doi.org/10.1016/j.oceaneng.2019.106716.

## References

An, C., Liu, H., Ren, Z., Yuan, Y., 2018. Prediction of tsunami waves by uniform slip models. J. Geophys. Res. Ocean. 123, 8366–8382.
An, C., Meng, L., 2017. Time reversal imaging of the 2015 Illapel tsunami source. Geophys. Res. Lett. 44, 1732–1739.
An, C., Sepúlveda, I., Liu, P.L.F., 2014. Tsunami source and its validation of the 2014 Iquique, Chile, earthquake. Geophys. Res. Lett. 41, 3988–3994.
An, C., Yue, H., Sun, J., Meng, L., Báez, J.C., 2017. The 2015 Mw 8.3 Illapel, Chile, earthquake: Direction-reversed along-dip rupture with localized water reverberation. Bull. Seismol. Soc. Am. 107, 2416–2426.
Blaser, L., Krüger, F., Ohrnberger, M., Scherbaum, F., 2010. Scaling relations of earthquake source parameter estimates with special focus on subduction environment. Bull. Seismol. Soc. Am. 100, 2914–2926.
Cisternas, M., Atwater, B.F., Torrejón, F., Sawai, Y., Machuca, G., Lagos, M., Eipert, A., Youlton, C., Salgado, I., Kamataki, T., et al., 2005. Predecessors of the giant 1960 Chile earthquake. Nature 437, 404.
Dziewonski, A.M., Anderson, D.L., 1981. Preliminary reference Earth model. Phys. Earth Planet. Inter. 25, 297–356.
Ekström, G., Nettles, M., Dziewoński, A., 2012. The global CMT project 2004–2010: Centroid-moment tensors for 13,017 earthquakes. Phys. Earth Planet. Inter. 200, 1–9.
Fujii, Y., Satake, K., Sakai, S., Shinohara, M., Kanazawa, T., 2011. Tsunami source of the 2011 off the Pacific coast of Tohoku earthquake. Earth Planets Space 63, 815–820.
Galgana, G., Hamburger, M., McCaffrey, R., Corpuz, E., Chen, Q., 2007. Analysis of crustal deformation in Luzon, Philippines using geodetic observations and earthquake focal mechanisms. Tectonophysics 432, 63–87.
Hayes, G.P., Wald, D.J., Johnson, R.L., 2012. Slab1. 0: A three-dimensional model of global subduction zone geometries. J. Geophys. Res. Solid Earth 117.
Heidarzadeh, M., Murotani, S., Satake, K., Ishibe, T., Gusman, A.R., 2016. Source model of the 16 September 2015 Illapel, Chile, Mw 8.4 earthquake based on teleseismic and tsunami data. Geophys. Res. Lett. 43, 643–650.
Hsu, Y.J., Yu, S.B., Song, T.R.A., Bacolcol, T., 2012. Plate coupling along the Manila subduction zone between Taiwan and northern Luzon. J. Asian Earth Sci. 51, 98–108.

Ichinose, G., Somerville, P., Thio, H.K., Graves, R., O'Connell, D., 2007. Rupture process of the 1964 Prince William Sound, Alaska, earthquake from the combined inversion of seismic, tsunami, and geodetic data. J. Geophys. Res. Solid Earth 112.
Kamigaichi, O., 2009. Tsunami forecasting and warning. In: Encyclopedia of Complexity and Systems Science. Springer, New York, pp. 9592–9618.
Kawai, H., Satoh, M., Kawaguchi, K., Seki, K., 2013. Characteristics of the 2011 Tohoku tsunami waveform acquired around Japan by NOWPHAS equipment. Coast. Eng. J. 55, 1350008.
Kido, M., Osada, Y., Fujimoto, H., Hino, R., Ito, Y., 2011. Trench-normal variation in observed seafloor displacements associated with the 2011 Tohoku-Oki earthquake. Geophys. Res. Lett. 38.
Kirby, J.T., Shi, F., Tehranirad, B., Harris, J.C., Grilli, S.T., 2013. Dispersive tsunami waves in the ocean: Model equations and sensitivity to dispersion and Coriolis effects. Ocean Model. 62, 39–55.
Lay, T., Ammon, C.J., Kanamori, H., Xue, L., Kim, M.J., 2011. Possible large near-trench slip during the 2011 Mw 9.0 off the Pacific coast of Tohoku earthquake. Earth Planets Space 63, 687–692.
Lay, T., Kanamori, H., Ammon, C.J., Nettles, M., Ward, S.N., Aster, R.C., Beck, S.L., Bilek, S.L., Brudzinski, M.R., Butler, R., et al., 2005. The great Sumatra-Andaman earthquake of 26 December 2004. Science 308, 1127–1133.
Lay, T., Yue, H., Brodsky, E.E., An, C., 2014. The 1 2014 Iquique, Chile, mw 8.1 earthquake rupture sequence. Geophys. Res. Lett. 41, 3818–3825.
Li, L., Lay, T., Cheung, K.F., Ye, L., 2016. Joint modeling of teleseismic and tsunami wave observations to constrain the 16 2015 Illapel, Chile, mw 8.3 earthquake rupture process. Geophys. Res. Lett. 43, 4303–4312.
Li, Z.S., Zhao, X., An, C., Liu, H., 2018. Wave profiles of a virtual extreme tsunami in the northern region of South China Sea. J. Earthq. Tsunami 12, 1840004.
Lin, S.C., Wu, T.R., Yen, E., Chen, H.Y., Hsu, J., Tsai, Y.L., Lee, C.J., Philip, L.F.L., 2015. Development of a tsunami early warning system for the South China Sea. Ocean Eng. 100, 1–18.
Liu, P.L.F., Wang, X., Salisbury, A.J., 2009. Tsunami hazard and early warning system in South China Sea. J. Asian Earth Sci. 36, 2–12.
Megawati, K., Shaw, F., Sieh, K., Huang, Z., Wu, T.R., Lin, Y., Tan, S.K., Pan, T.C., 2009. Tsunami hazard from the subduction megathrust of the South China Sea: Part I. source characterization and the resulting tsunami. J. Asian Earth Sci. 36, 13–20.
Melgar, D., Fan, W., Riquelme, S., Geng, J., Liang, C., Fuentes, M., Vargas, G., Allen, R.M., Shearer, P.M., Fielding, E.J., 2016. Slip segmentation and slow rupture to the trench during the 2015, Mw8.3 Illapel, Chile earthquake. Geophys. Res. Lett. 43, 961–966.
Melgar, D., Williamson, A.L., Salazar-Monroy, E.F., 2019. Differences between heterogenous and homogenous slip in regional tsunami hazards modelling. Geophys. J. Int. 219, 553–562.
Murotani, S., Miyake, H., Koketsu, K., 2008. Scaling of characterized slip models for plate-boundary earthquakes. Earth Planets Space 60, 987–991.
Murotani, S., Satake, K., Fujii, Y., 2013. Scaling relations of seismic moment, rupture area, average slip, and asperity size for M9̃ subduction-zone earthquakes. Geophys. Res. Lett. 40, 5070–5074.
Nguyen, P.H., Bui, Q.C., Vu, P.H., Pham, T.T., 2014. Scenario-based tsunami hazard assessment for the coast of Vietnam from the Manila Trench source. Phys. Earth Planet. Inter. 236, 95–108.
NOAA, 2019. NGDC/WDS global historical tsunami database. url: https://www.ngdc.noaa.gov/hazard/tsu_db.shtml. http://dx.doi.org/10.7289/V5PN93H7. (Accessed: 2019-09-30).
Okada, Y., 1985. Surface deformation due to shear and tensile faults in a half-space. Bull. Seismol. Soc. Am. 75, 1135–1154.
Reimnitz, E., Marshall, N.F., 1965. Effects of the Alaska earthquake and tsunami on recent deltaic sediments. J. Geophys. Res. 70, 2363–2376.
Ren, Z.Y., Liu, H., Wang, B.L., Zhao, X., 2014. An investigation on multi-buoy inversion method for tsunami warning system in South China Sea. J. Earthq. Tsunami 8, 1440004.
Ren, Z., Liu, H., Zhao, X., Wang, B., An, C., 2019. Effect of kinematic fault rupture process on tsunami propagation. Ocean Eng. 181, 43–58.
Ren, Z.Y., Zhao, X., Liu, H., 2015. Dispersion effects on tsunami propagation in South China Sea. J. Earthq. Tsunami 9, 1540001.
Ren, Z.y., Zhao, X., Wang, B.l., Dias, F., Liu, H., 2017. Characteristics of wave amplitude and currents in South China Sea induced by a virtual extreme tsunami. J. Hydrodyn. 29, 377–392.
Satake, K., 1987. Inversion of tsunami waveforms for the estimation of a fault heterogeneity: Method and numerical experiments. J. Phys. Earth 35, 241–254.
Satake, K., Fujii, Y., Harada, T., Namegaya, Y., 2013. Time and space distribution of coseismic slip of the 2011 Tohoku earthquake as inferred from tsunami waveform data. Bull. Seismol. Soc. Am. 103, 1473–1492.
Shi, F., Kirby, J.T., Harris, J.C., Geiman, J.D., Grilli, S.T., 2012. A high-order adaptive time-stepping TVD solver for Boussinesq modeling of breaking waves and coastal inundation. Ocean Model. 43, 36–51.
Simons, M., Minson, S.E., Sladen, A., Ortega, F., Jiang, J., Owen, S.E., Meng, L., Ampuero, J.P., Wei, S., Chu, R., et al., 2011. The 2011 magnitude 9.0 Tohoku-Oki earthquake: Mosaicking the megathrust from seconds to centuries. Science 332, 1421–1425.
Stirling, M., Goded, T., Berryman, K., Litchfield, N., 2013. Selection of earthquake scaling relationships for seismic-hazard analysis. Bull. Seismol. Soc. Am. 103, 2993–3011.
Strasser, F., Arango, M., Bommer, J., 2010. Scaling of the source dimensions of interface and intraslab subduction-zone earthquakes with moment magnitude. Seismol. Res. Lett. 81, 941–950.
Thingbaijam, K.K.S., Martin Mai, P., Goda, K., 2017. New empirical earthquake source-scaling laws. Bull. Seismol. Soc. Am. 107, 2225–2246.
Tilmann, F., Zhang, Y., Moreno, M., Saul, J., Eckelmann, F., Palo, M., Deng, Z., Babeyko, A., Chen, K., Baez, J., et al., 2016. The 2015 Illapel earthquake, central Chile: A type case for a characteristic earthquake? Geophys. Res. Lett. 43, 574–583.
Titov, V., Rabinovich, A.B., Mofjeld, H.O., Thomson, R.E., González, F.I., 2005. The global reach of the 26 2004 Sumatra tsunami. Science 309, 2045–2048.
Wei, Y., Bernard, E.N., Tang, L., Weiss, R., Titov, V.V., Moore, C., Spillane, M., Hopkins, M., Kânoğlu, U., 2008. Real-time experimental forecast of the Peruvian tsunami of August 2007 for US coastlines. Geophys. Res. Lett. 35.
Wei, Y., Cheung, K.F., Curtis, G.D., McCreery, C.S., 2003. Inverse algorithm for tsunami forecasts. J. Waterway Port Coast. Ocean Eng. 129, 60–69.
Wells, D.L., Coppersmith, K.J., 1994. New empirical relationships among magnitude, rupture length, rupture width, rupture area, and surface displacement. Bull. Seismol. Soc. Am. 84, 974–1002.
Wu, T.R., Huang, H.C., 2009. Modeling tsunami hazards from Manila trench to Taiwan. J. Asian Earth Sci. 36, 21–28.